Behaviour of the Serre Equations in the Presence of Steep Gradients Revisited

J.P.A. Pitt[a,*], C. Zoppou[a], S.G. Roberts[a]

[a] *Mathematical Sciences Institute, Australian National University, Canberra, ACT 0200, Australia*

Abstract

Keywords: Serre equations, steep gradients, dam break

1. Numerical Results

We begin by looking into the effect of the initial steepness of the smoothed dam-break problem for different α values by observing what happens as $\Delta x \to 0$ and our numerical solutions better approximate the true solution of the Serre equations. We then investigate numerical results for long time scales and how the shallow water wave equations analytic solution and El's Whitham modulation values compare to our numerical solutions.

All numerical methods used $\Delta t = 0.01\Delta x$ which is smaller than required by the CFL condition [1] which ensures stability of our schemes. The time step Δt was chosen to be smaller than necessary because for a final time of $t = 30s$ making Δt small suppresses errors without excessively increasing the run-time of the experiments. The method $\mathcal{V}_2$ requires an input parameter to its slope limiter and this was chosen to be $\theta = 1.2$ [2]. All of the numerical methods presented use Dirichlet boundary conditions with $u = 0m/s$ at both boundaries and $h = 1.8m$ on the left and $h = 1m$ on the right.

1.1. Observed Structures of the Numerical Solutions

We observe that there are four different structures as $\Delta x \to 0$ depending on the α and the numerical method. They are the non-oscillatory structure, the flat structure, the node structure and the growth structure. An example of each of these structures is in Figure 1 for $\mathcal{V}_3$'s numerical solutions of various smoothed dam-break problems.

The four structures are identified by the nature of the numerical solutions in regions III and IV when Δx is small and they correspond to different structures in the numerical solutions presented in the literature. From Figure 1 it can be seen that as α is decreased, steepening the initial conditions the numerical solutions demonstrate an increase in the size and number of oscillations particularly around x_{u_2}.

*Corresponding author

Email addresses: jordan.pitt@anu.edu.au (J.P.A. Pitt), christopher.zoppou@anu.edu.au (C. Zoppou), stephen.roberts@anu.edu.au (S.G. Roberts)

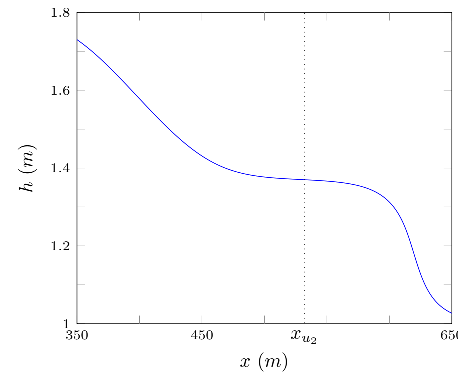

Non-oscillatory structure (α = 40m)

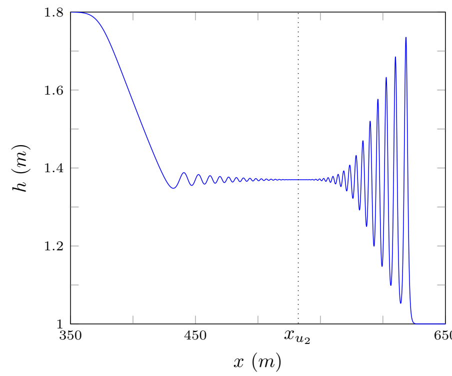

Flat structure (α = 2m)

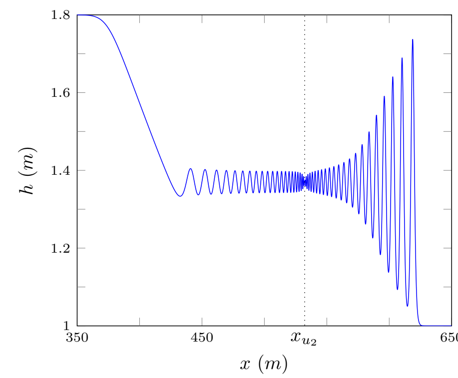

Node structure (α = 0.4m)

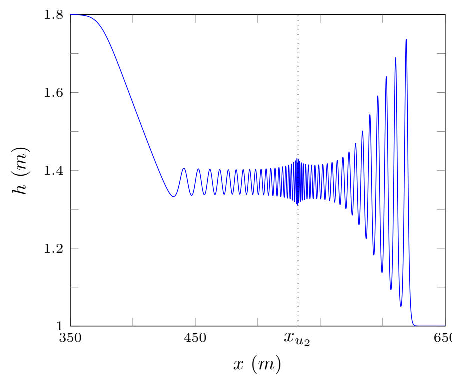

Growth structure (α = 0.1m)

Figure 1: Numerical results of $\mathcal{V}_3$ with $\Delta x = 10/2^{11}m$ (—) at $t = 30s$ for various smooth dam-break problems demonstrating the different observed structures.

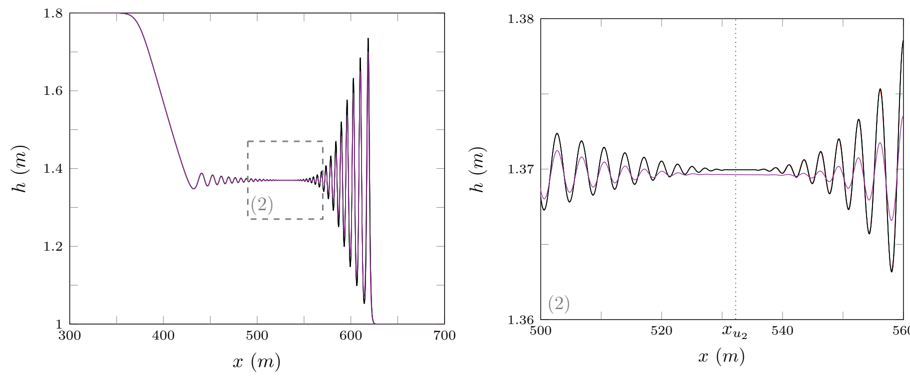

Figure 2: Numerical solutions $\mathcal{E}$ (—), $\mathcal{G}$ (—), $\mathcal{V}_3$ (—), $\mathcal{V}_2$ (—) and $\mathcal{V}_1$ (—) with $\Delta x = 10/2^{11}m$ at $t = 30s$ for the smooth dam-break problem with $\alpha = 2m$.

For the non-oscillatory and flat structures there is excellent agreement between all higher-order numerical methods at our highest resolution $\Delta x = 10/2^{11}m$. An illustration of this agreement is given in Figure 2 for the flat structure. Since the first-order scheme is diffusive [2] we find that although it's highest resolution numerical solution has the same behaviour as the other methods it damps the oscillations. Because our numerical solutions to the smoothed dam-break problems with $\alpha = 40m$ and $\alpha = 2m$ from different methods agree at our highest resolution the investigation of the behaviour of numerical solutions as $\Delta x \to 0$ for these smoothed dam-break problems will use $\mathcal{V}_3$ exclusively.

1.1.1. Non-oscillatory Structure

The first structure is the non-oscillatory structure it is the result of a large α. When α is large for the smoothed dam-break problem the fluid to the left of x_0 flows to fill the right side, but due to the large α the front of this flow is not steep enough to generate undulations over short time spans. Eventually the front of this flow steepens due to non-linearity and undulations develop there.

This structure is not present in the literature as no authors chose large enough α. An example of this structure can be seen in Figure 3 for $\alpha = 40m$ using $\mathcal{V}_3$. Because this is a very smooth problem we observe that all numerical results are visually identical for all $\Delta x < 10/2^4 m$.

From Table 1 it can be seen that not only have these solutions converged visually but the L_1 measures demonstrate that we have reached convergence to round-off error by $\Delta x = 10/2^8 m$ after which the relative difference between numerical solutions plateau.

Table 1 also demonstrates that the error in conservation of the numerical solutions are at round-off error for h and $\mathcal{H}$. C_1^{uh} is the worst performing of the measures because the smoothed dam-break has such a large α that $h(0m) \neq 1.8m$ and $h(1000m) \neq 1m$ causing unequal fluxes in momentum at the boundaries.

The convergence and conservation of numerical solutions as $\Delta x \to 0$ together with the agreement of different numerical methods methods demonstrates that the numerical result in Figure 3 and its non-oscillatory structure is an accurate representation of the

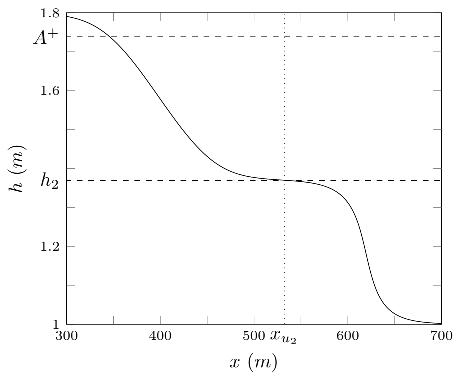

Figure 3: Numerical results of $\mathcal{V}_3$ at $t = 30s$ for smooth dam-break problem with $\alpha = 40m$ for $\Delta x = 10/2^{10}m$ (—), $10/2^8m$ (—), $10/2^6m$ (—) and $10/2^4m$ (—).

solutions of the Serre equations when α is sufficiently large and in particular $\alpha = 40m$.

1.1.2. Flat Structure

The second structure will be referred to as the flat structure due to the presence of a constant height around x_{u_2}, this is the most common structure observed in the literature [3, 4, 5]. It is generated as are the rest of the methods when the initial conditions are steep enough such that the bore that develops has undulations. This structure consists of oscillations in regions III and IV which are separated by a constant height state around x_{u_2}. An example of the structure can be seen in the numerical solutions presented in Figure 4 when $\alpha = 2m$.

As Δx decreases the numerical solutions converge so that by $\Delta x = 10/2^8m$ the solutions for higher Δx are visually identical. Table 1 demonstrates that although we have convergence visually the L_1 measures are still decreasing and haven't plateaued. Likewise the C_1 are still decreasing and have only reached round-off error for h, although our numerical solutions do exhibit good conservation. This indicates that to precisely resolve the numerical solutions for $\mathcal{V}_3$ of this smoothed dam-break problem down to round-off error would require an even lower Δx.

The convergence of our numerical solutions as $\Delta x \to 0$ of $\mathcal{V}_3$ both in Figure 4 and Table 1 as well as the agreement of all the models in Figure 2 with $\Delta x = 10/2^{11}m$ demonstrates that while our solutions have not converged down to round-off error our numerical solutions are very accurate solutions of the Serre equations for the smoothed dam-break problem with $\alpha = 0.5m$.

These numerical solutions compare well with those of Mitsotakis et al. [4] who use the same α but different h_0 and h_1 and resolve the same behaviour. We found that we resolved this structure for all methods at $\Delta x = 10/2^{11}m$ for the smoothed dam-break with α's as low as $1m$. This is the same behaviour that is present in the numerical solutions of Mitsotakis et al. [5] who use $\alpha = 1m$ but different heights. Therefore Mitsotakis et al. [4] and Mitsotakis et al. [5] only observe the flat scenario in their numerical results due to their choice of α for the smoothed dam-break problem.

α	Δx	C_1^h	C_1^{uh}	$C_1^{\mathcal{H}}$	L_1^h	L_1^u
40	$10/2^4$	$12 \cdot 10^{-11}$	$1.77 \cdot 10^{-6}$	$1.23 \cdot 10^{-8}$	$1.74 \cdot 10^{-7}$	$2.90 \cdot 10^{-6}$
40	$10/2^6$	$1.07 \cdot 10^{-11}$	$1.50 \cdot 10^{-6}$	$1.49 \cdot 10^{-10}$	$2.57 \cdot 10^{-9}$	$4.19 \cdot 10^{-8}$
40	$10/2^8$	$8.77 \cdot 10^{-13}$	$5.49 \cdot 10^{-7}$	$3.77 \cdot 10^{-13}$	$6.08 \cdot 10^{-11}$	$5.28 \cdot 10^{-10}$
40	$10/2^{10}$	$1.77 \cdot 10^{-11}$	$2.21 \cdot 10^{-8}$	$3.56 \cdot 10^{-11}$	$2.54 \cdot 10^{-11}$	$6.49 \cdot 10^{-11}$
2	$10/2^4$	$4.9 \cdot 10^{-14}$	$5.10 \cdot 10^{-3}$	$8.69 \cdot 10^{-4}$	$5.02 \cdot 10^{-3}$	$6.77 \cdot 10^{-2}$
2	$10/2^6$	$2.51 \cdot 10^{-13}$	$2.18 \cdot 10^{-4}$	$6.58 \cdot 10^{-5}$	$4.14 \cdot 10^{-4}$	$5.20 \cdot 10^{-3}$
2	$10/2^8$	$9.81 \cdot 10^{-13}$	$7.72 \cdot 10^{-7}$	$5.01 \cdot 10^{-7}$	$6.00 \cdot 10^{-6}$	$7.59 \cdot 10^{-5}$
2	$10/2^{10}$	$3.95 \cdot 10^{-12}$	$5.56 \cdot 10^{-9}$	$6.13 \cdot 10^{-9}$	$1.76 \cdot 10^{-7}$	$2.33 \cdot 10^{-6}$
0.4	$10/2^4$	$9 \cdot 10^{-14}$	$4.82 \cdot 10^{-3}$	$1.02 \cdot 10^{-3}$	$6.79 \cdot 10^{-3}$ †	$9.93 \cdot 10^{-2}$ †
0.4	$10/2^6$	$2.4 \cdot 10^{-13}$	$2.41 \cdot 10^{-4}$	$1.11 \cdot 10^{-4}$	$8.89 \cdot 10^{-4}$ †	$1.13 \cdot 10^{-2}$ †
0.4	$10/2^8$	$9.68 \cdot 10^{-13}$	$7.57 \cdot 10^{-7}$	$2.25 \cdot 10^{-6}$	$1.53 \cdot 10^{-5}$ †	$1.91 \cdot 10^{-4}$ †
0.4	$10/2^{10}$	$3.91 \cdot 10^{-12}$	$4.95 \cdot 10^{-9}$	$2.01 \cdot 10^{-8}$	$3.61 \cdot 10^{-7}$ †	$5.00 \cdot 10^{-6}$ †
0.1	$10/2^4$	$7.6 \cdot 10^{-14}$	$4.82 \cdot 10^{-3}$	$1.06 \cdot 10^{-3}$	$7.04 \cdot 10^{-3}$ †	$1.02 \cdot 10^{-1}$ †
0.1	$10/2^6$	$2.4 \cdot 10^{-13}$	$2.39 \cdot 10^{-4}$	$1.44 \cdot 10^{-4}$	$1.02 \cdot 10^{-3}$ †	$1.28 \cdot 10^{-2}$ †
0.1	$10/2^8$	$9.79 \cdot 10^{-13}$	$2.21 \cdot 10^{-7}$	$1.20 \cdot 10^{-5}$	$2.86 \cdot 10^{-5}$ †	$3.46 \cdot 10^{-4}$ †
0.1	$10/2^{10}$	$3.92 \cdot 10^{-12}$	$4.46 \cdot 10^{-8}$	$7.61 \cdot 10^{-7}$	$4.99 \cdot 10^{-7}$ †	$6.40 \cdot 10^{-6}$ †

Table 1: All errors in conservation C_1^q (**??**) for the conserved quantities and relative distances L_1^q (**??**) of the primitive variables for numerical solutions of $\mathcal{V}_3$. L_1^q uses the numerical solution with $\Delta x = 10/2^{11}m$ as the high resolution basis of comparison and † indicates the omission of the interval $[520m, 540m]$ from the comparison.

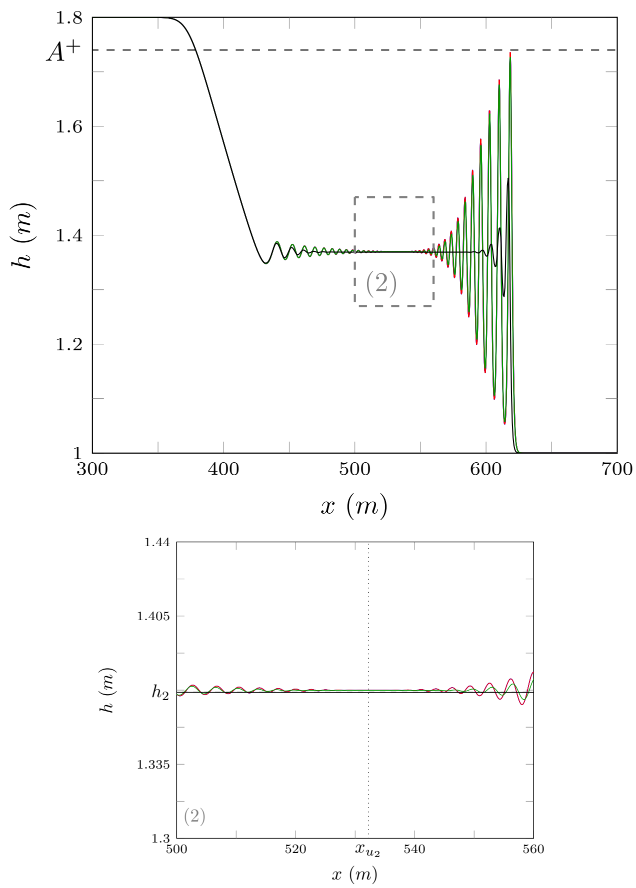

Figure 4: Numerical results of $\mathcal{V}_3$ at $t = 30s$ for the smooth dam-break problem with $\alpha = 2m$ for $\Delta x = 10/2^{10}m$ (—), $10/2^8m$ (—), $10/2^6m$ (—) and $10/2^4m$ (—).

The first-order $\mathcal{V}_1$ is diffusive [2] and damps oscillations that are present in higher-order methods numerical results as in Figure 2. We find that for any $\alpha \leq 4m$ and the discontinuous dam-break problem our numerical solutions of $\mathcal{V}_1$ at $t = 30s$ with $\Delta x = 10/2^{11}m$ can only resolve the flat scenario which can be seen in Figure 5 for $\alpha = 0.001m$. Therefore Le Métayer et al. [3] using $\mathcal{V}_1$ with their chosen Δx and Δt which is lower than the ones used in this paper could only resolve the flat structure as well.

1.1.3. Node Structure

The third structure will be referred to as the node structure and it is was observed by [6]. The node structures main feature is that the oscillations in region III and IV decay and appear to meet at x_{u_2} as can be seen in Figure 6 when $\alpha = 0.4m$.

Figure 6 demonstrates that our numerical solutions have not converged, however this is only in the area around x_{u_2}. Due to the large difference in numerical solutions around x_{u_2} the L_1 measure over the area around x_{u_2} would not be insightful, however by

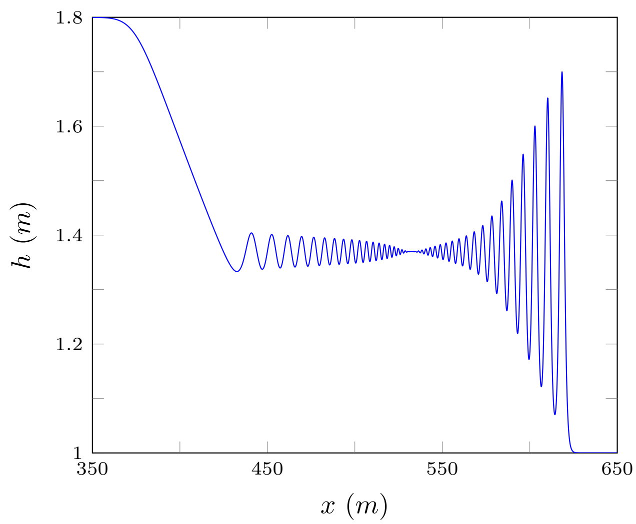

Figure 5: Numerical solution of $\mathcal{V}_1$ at $t = 30s$ for the smooth dam-break problem with $\alpha = 0.001m$ for $\Delta x = 10/2^{11}m$ (—).

omitting this region we can gain some knowledge about how well our solutions agree away from x_{u_2}. This was performed for the relevant L_1 measures in Table 1 by omitting the interval $[520m,\ 540m]$. These modified L_1 measures demonstrate that while our numerical results have visually converged away from x_{u_2} they have not fully converged down to round-off error under the L_1 measure although they are close to one another.

Table 1 demonstrates that the C_1 measures are decreasing as well and have only reached round-off error for h. Therefore to resolve the numerical solution of this particular smoothed dam-break problem down to round-off error would require even lower Δx values.

There is a good agreement across different numerical methods for $\Delta x = 10/2^{11}m$ as can be seen in Figure 7. In particular all the higher-order methods exhibit the same behaviour and most only disagree in a very small region around x_{u_2}, although we observe that $\mathcal{G}$ which we found to introduce the largest errors has not converged as well to the numerical solutions of the other methods.

The behaviour of $\mathcal{V}_3$'s solutions as $\Delta x \to 0$ and the agreement of different numerical methods when $\Delta x = 10/2^{11}m$ in particular $\mathcal{V}_3$, $\mathcal{V}_2$ and $\mathcal{E}$ demonstrate that while our numerical solutions have not completely visually converged they are an accurate representation of the solutions of the Serre equations for the smoothed dam-break problem with $\alpha = 0.4m$. In particular for $\alpha = 0.4m$ the node structure should be observed in numerical solutions of the Serre equations.

These numerical solutions support the findings of El et al. [6] who also use some smoothing [7] but do not report what smoothing was performed. Using their method $\mathcal{G}$ and similar Δx to El et al. [6] we are able to resolve the growth behaviour for smaller α's, indicating that the smoothing performed by El et al. [6] limited their observed behaviour to just the node structure.

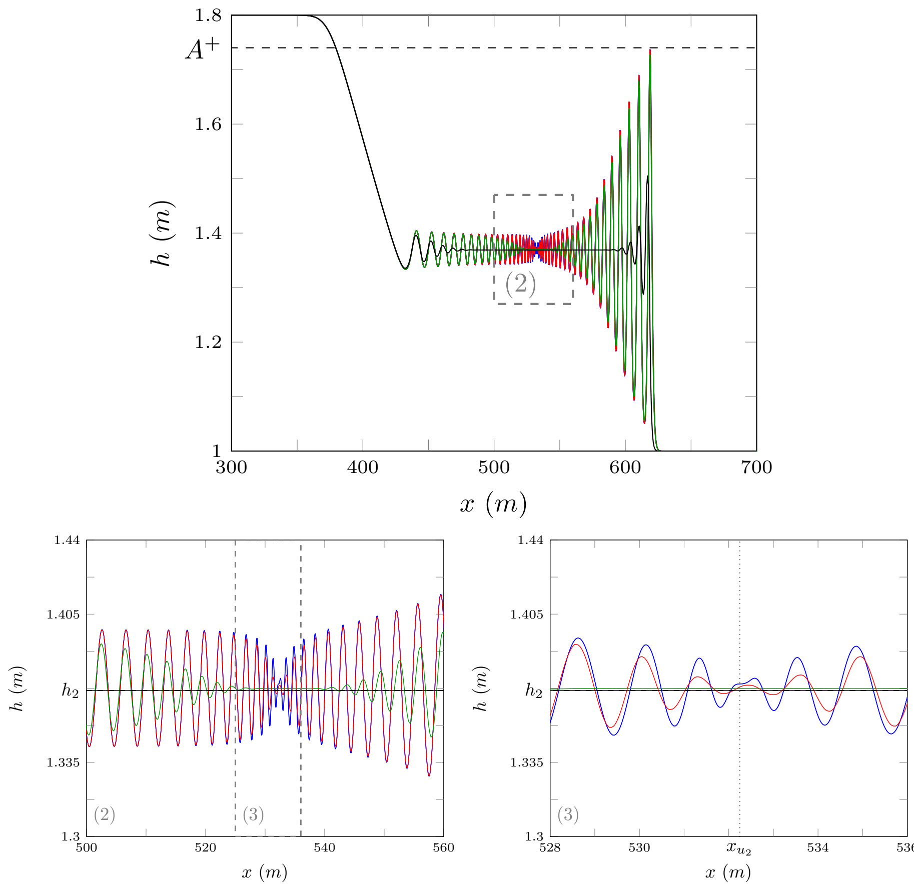

Figure 6: Numerical solution of $\mathcal{V}_3$ at $t = 30s$ for the smooth dam-break problem with $\alpha = 0.4m$ for $\Delta x = 10/2^{10}m$ (—), $10/2^{8}m$ (—), $10/2^{6}m$ (—) and $10/2^{4}m$ (—).

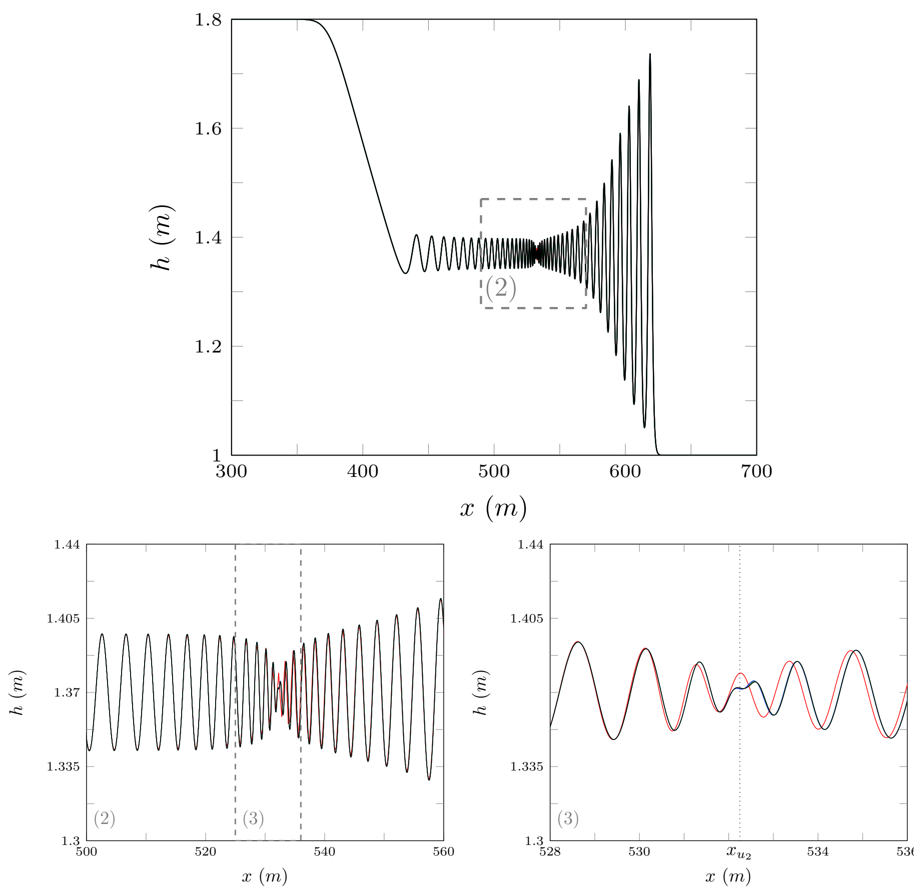

Figure 7: Numerical solution of $\mathcal{E}$ (—), $\mathcal{G}$ (—), $\mathcal{V}_3$ (—) and $\mathcal{V}_2$ (—) at $t = 30s$ with $\Delta x = 10/2^{11}m$ for the smoothed dam-break problem with $\alpha = 0.4m$.

1.1.4. Growth Structure

The fourth structure is the growth structure which has hitherto not been published. It features a growth in the oscillation amplitude around x_{u_2}. An example of the growth structure can be seen for $\mathcal{V}_3$'s numerical solutions in Figure 8 of the smoothed dam-break problem with $\alpha = 0.1m$. This structure was observed in the numerical solutions of $\mathcal{V}_3$ for $\Delta x = 10/2^{11}m$ at $t = 30s$ for α's as low as $0.001m$ and even for the discontinuous dam-break problem.

Figure 8 shows that this behaviour can only be observed for $\Delta x = 10/2^{10}m$, with poor convergence of the numerical results around x_{u_2}. Thus our L_1 measures in Table 1 omit the interval $[520m, 540m]$ to compare the numerical solutions. This demonstrates that away from x_{u_2} our numerical solutions are quite close to one another but they have not converged to round-off error as $\Delta x \to 0$. The C_1 measures in Table 1 are still decreasing and have only attained round-off error for h, although for uh and $\mathcal{H}$ the errors in conservation are still small. These measures continue the trend in Table 1 where smaller α's and thus steeper initial conditions lead to large relative distance between numerical solutions and poorer convergence because they are more difficult to solve accurately.

Figure 9 demonstrates that our numerical solutions for $\Delta x = 10/2^{11}m$ with the best methods $\mathcal{E}$, $\mathcal{V}_3$ and $\mathcal{V}_2$ disagree for only a few oscillations around x_{u_2}. Since both $\mathcal{G}$ and $\mathcal{E}$ are second-order finite difference methods their errors are dispersive meaning that oscillation size and number in their numerical solutions are overestimated, as can be seen for the large dispersive errors of $\mathcal{G}$. All $\mathcal{V}_i$ methods are diffusive and therefore underestimate the size and number of oscillations in their numerical solutions. Therefore the true solution of the Serre equations should be between the dispersive method $\mathcal{E}$ and the diffusive method $\mathcal{V}_3$ which is a growth structure.

These results then indicate that the solutions of the Serre equations to the smoothed dam-break with sufficiently small α's should exhibit a growth structure at $t = 30s$, even though we have not precisely resolved all the oscillations in our numerical solutions.

It was found that decreasing α did increase the amplitude of the oscillations around x_{u_2} but not drastically and for $\mathcal{V}_3$ with $\Delta x = 10/2^{11}m$ and $\alpha = 0.001m$ the oscillations occurred within the interval $[1.28m, 1.46m]$. Of particular note is that the number of oscillations are the same in Figures 7 and 9 for the best methods even though they have different structures.

1.2. Shallow water wave equation comparison

The analytic solutions of shallow water wave equations have been used as a guide for the mean behaviour of the solution of the Serre equations for the dam-break problem in the literature [3, 4].

To assess the applicability of this the mean of our numerical solution of u and h in the interval $[x_{u_2} - 50m, x_{u_2} + 50m]$ were calculated for a range of different smoothed dam-break height ratios and compared to their respective approximation from the shallow water wave equations u_2 and h_2. The results of this can be seen in Figure 10 for numerical solutions of $\mathcal{V}_3$ where $\Delta x = 10/2^{10}m$ and $t = 100s$ for the smoothed dam-break with $\alpha = 0.1m$ where h_0 is fixed and h_1 is varied. It can be seen that although these results are not precise the values h_2 and u_2 are good approximations to the mean behaviour of the fluid inside the bore for a range of different aspect ratios.

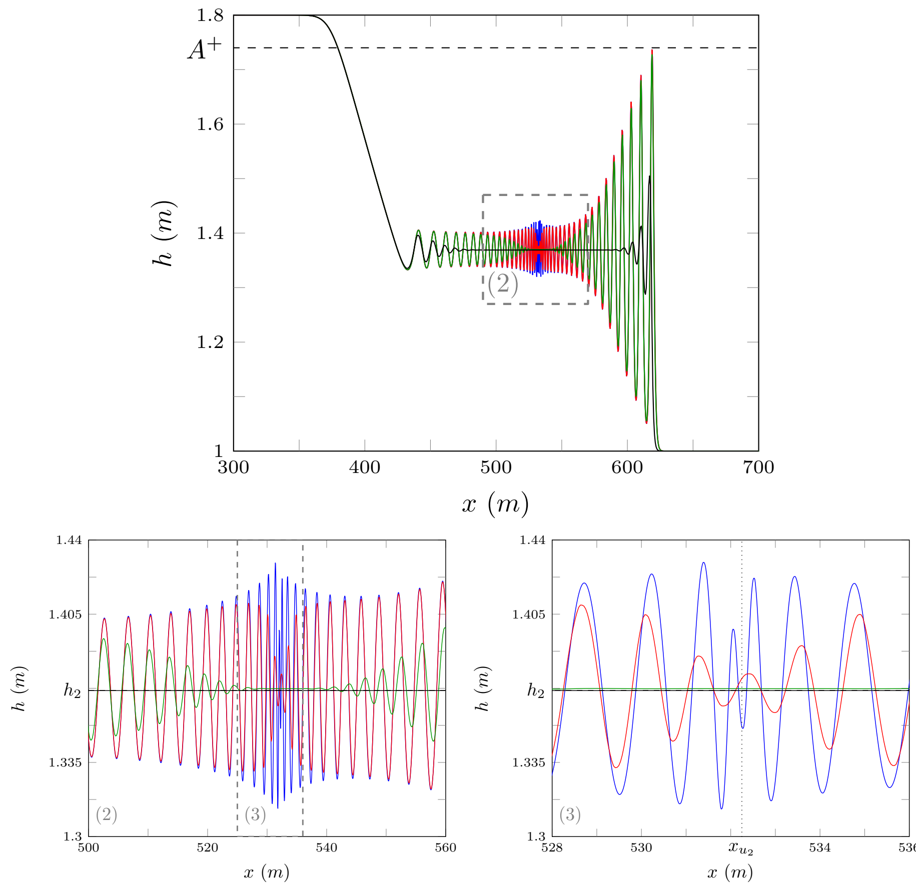

Figure 8: Numerical solutions of $\mathcal{V}_3$ at $t = 30s$ for the smooth dam-break problem with $\alpha = 0.1m$ for $\Delta x = 10/2^{10}m$ (—), $10/2^8m$ (—), $10/2^6m$ (—) and $10/2^4m$ (—).

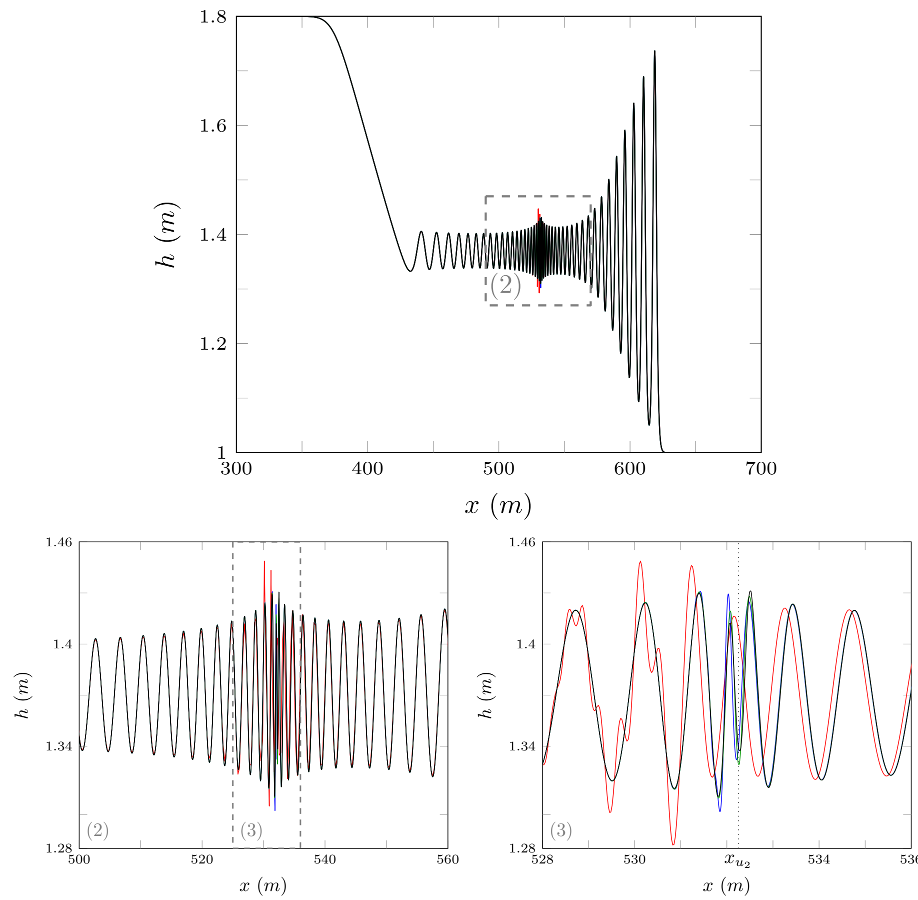

Figure 9: Numerical solutions of $\mathcal{E}$ (—), $\mathcal{G}$ (—), $\mathcal{V}_3$ (—) and $\mathcal{V}_2$ (—) at $t = 30s$ with $\Delta x = 10/2^{11}m$ for the smoothed dam-break problem with $\alpha = 0.1m$.

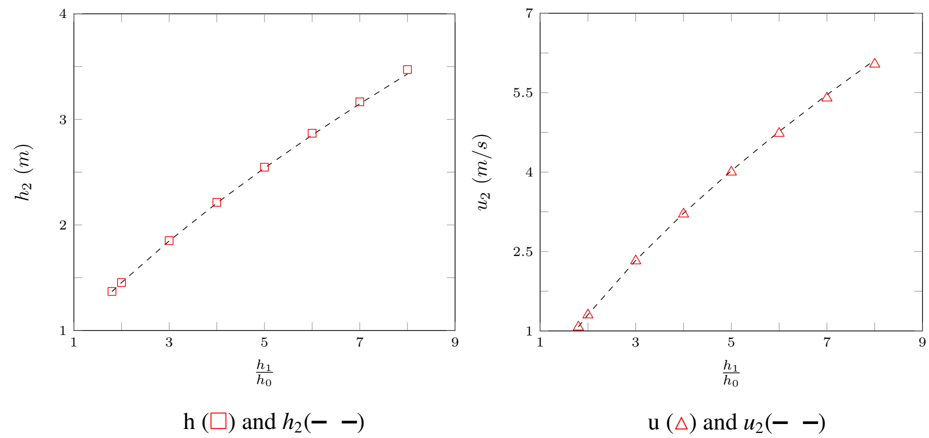

Figure 10: Comparison between mean behaviour of the Serre equations and the values of the analytic solution of the shallow water wave equations that approximate them for a range of different aspect ratios.

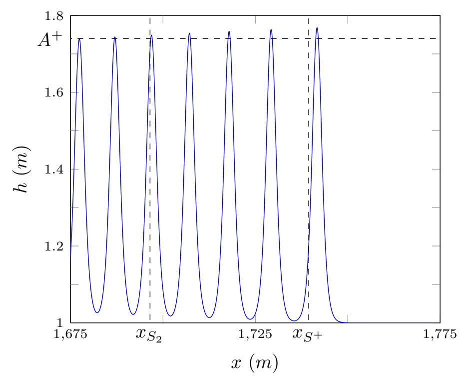

Figure 11: Oscillations at the front of undular bore for numerical solutions of $\mathcal{V}_3$ of the Serre equations for the smoothed dam-break with $\alpha = 0.1m$ at $t = 300s$.

The location of the front of the bore predicted by the shallow water wave equations x_{S_2} is however not a good approximation to the front of the undular bore of the Serre equations as can be seen for $\mathcal{V}_3$'s numerical solution to the smoothed dam-break problem with $\alpha = 0.1m$ at $t = 300s$ in Figure 10.

1.3. Whitham modulation comparison

The expressions for the leading wave amplitude A^+ and speed S^+ obtained by [6] are asymptotic results and so we are interested in how our numerical results behave over time. Thus for the smoothed dam-break problem with $\alpha = 0.1m$ the peak amplitude in region IV (A) was plotted over time in Figure 12. It can seen that A approaches a value larger than A^+ over time. We find that as $\alpha \to 0$ and $\Delta x \to 0$ A converges away from A^+ in this time scale for this aspect ratio. Thus it appears that the true solution of the dam-break for the Serre equations has an amplitude in region IV slightly above A^+. This is not inconsistent with the results of [6] as their scale comparing A^+ to A is too large to see such a small difference.

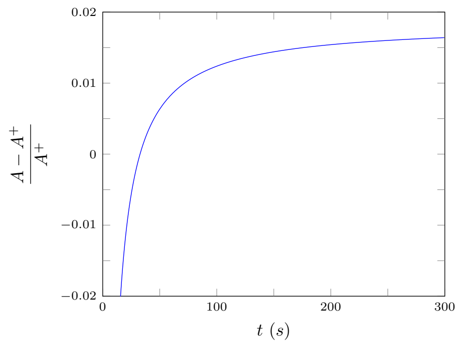

Figure 12: Relative error between wave height A and A^+ plotted over time for the numerical solution of the smooth dam-break problem by $\mathcal{V}_3$ with $\alpha = 0.1m$ for $\Delta x = 10/2^9 m$ (—).

S^+ is strongly related to A^+ and so a plot like Figure 12 for it is extraneous. In Figure 11 it can be seen that the location of the initial wave predicted by S^+, x_{S^+} is a slight underestimate although it is a better prediction than x_{S_2}.

[1] A. A. Harten, High resolution schemes for hyperbolic conservation laws, Journal of Computational Physics 49 (3) (1983) 357–393.

[2] C. Zoppou, J. Pitt, S. Roberts, Numerical Solution of the Fully Non-linear Weakly Dispersive Serre Equations for Steep Gradient Flows, Applied Mathematical Modelling 00 (00) (2017) 00–00.

[3] O. Le Métayer, S. Gavrilyuk, S. Hank, A numerical scheme for the GreenNaghdi model, Journal of Computational Physics 229 (6) (2010) 2034–2045.

[4] D. Mitsotakis, B. Ilan, D. Dutykh, On the Galerkin/Finite-Element Method for the Serre Equations, Journal of Scientific Computing 61 (1) (2014) 166–195.

[5] D. Mitsotakis, D. Dutykh, J. Carter, On the nonlinear dynamics of the traveling-wave solutions of the Serre system, Wave Motion 70 (1) (2017) 166–182.

[6] G. El, R. H. J. Grimshaw, N. F. Smyth, Unsteady undular bores in fully nonlinear shallow-water theory, Physics of Fluids 18 (027104).

[7] G. El, M. Hoefer, Dispersive shock waves and modulation theory, Physica D: Nonlinear Phenomena 333 (2016) 11–65.